Structure, Motion, and Exchange Coupling of $^{15}NO_2/^{15}NO_2$ Radical Pairs Occupying Adjacent Solvent Cavities of α-HNIW, a Nitramine Hydrate

Lev R. Ryzhkov[†] and J. Michael McBride*

Contribution from the Department of Chemistry, Yale University, New Haven, Connecticut 06520-8107

Received September 9, 1996[⊗]

Abstract: Low-temperature photolysis of α-HNIW (2,4,6,8,10,12-hexanitrohexaazatetracyclo[5.5.0^{5,9}.0^{3,11}]dodecane) generated three $^{15}NO_2/^{15}NO_2$ radical pairs that were studied by single-crystal electron paramagnetic resonance spectroscopy at 80 K. In two of the pairs, A and B, the two NO_2 molecules occupy solvent cavities that are related by unit translation along the *a*-axis of the α-HNIW unit cell (radical pair separations of 9.26 and 9.67 Å). In the third pair, C, they occupy cavities related by translation along the *b*-axis (∼13 Å). Pair formation was highly specific since no pairs were trapped in cavities related by the *b*-glide (8.14 Å). All three observed pairs survived annealing to 215 K, but from 220 to 294 K they decayed, one by one, without interconverting or separating to isolated radicals. Positive and negative exchange couplings as large as 0.004 cm^{-1} were estimated through approximate simulation of the position and intensity of transitions involving the nuclear states with hyperfine-induced S_o-T_o mixing. Pairs B and C seem each to exist in two forms with a single NO_2/NO_2 structure but different values of *J*, due perhaps to different arrangement of nonbonded molecules between the radicals. Implications for the mechanism of solid-state HNIW decomposition and the limited mobility of small molecules in lightly damaged crystals are discussed.

Introduction

Because the tetracyclic hexanitramine HNIW[1] shows promise as a solid propellant and explosive, there is interest in the nature of its solid-state decomposition. Toscano has shown that photolyzing the α crystalline polymorph of HNIW at 337 nm and 20 K generates a complex EPR spectrum that simplifies upon annealing.[2] After annealing to 210 K a strong triplet signal of NO begins to appear, and by 300 K the original complex spectrum has disappeared and a signal due to NO_2 becomes sharper and stronger.

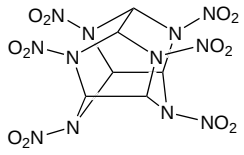

HNIW

The α polymorph of HNIW is a hydrate in which each HNIW molecule is adjacent to three symmetry-related cavities, each of which contains a disordered water molecule.[3] Toscano showed that the strong NO and NO_2 signals are due to well-ordered molecules trapped in water cavities of the single crystal. He further suggested that their growth at high temperature results from increased mobility that allows disordered radicals to diffuse and find previously vacant cavities, where they lodge permanently. This plausible suggestion contrasts with new evidence, reported below, suggesting very limited mobility.

Pace confirmed Toscano's findings for cavity-trapped NO_2, and went further to assign some peaks in the complex pre-annealing spectrum to a different orientation of NO_2.[4] The purpose of the present work was to characterize these low-temperature intermediates more thoroughly. They are in fact due to NO_2/NO_2 radical pairs.

Although most EPR studies of damaged organic solids have concerned isolated radicals, homolytic decompositions initially produce radical pairs. In these more primitive reaction intermediates the two radicals interact both magnetically, giving rise to zero-field splitting (zfs), and electrostatically, giving rise to exchange coupling (*J*). ZFS can be interpreted to supply the distance and direction between the radicals, and thus it provides detailed information about short-range translational mobility in the damaged solid. In the case of α-HNIW, zfs reveals remarkable specificity in the motion of NO_2/NO_2 pairs.

Intermolecular exchange coupling, *J*, measures the electrostatic energy difference between the singlet and triplet states of a radical pair.[5] Although *J* is closely related to such important processes as electron and excitation transfer[6] and bulk magnetism,[7] it is not easy to predict or calculate. The magnitude, and less often the sign, of *J* has been measured in a number of systems, but most of them involve a continuous chain of covalent or coordinate bonds between the paramagnetic centers,[8] where the contributions of through-space and through-bond coupling are difficult to separate.[9] When *J* of a flexible diradical or a radical pair is used as a fitting parameter for polarized

[†] Present address: Department of Chemistry, Towson State University, Baltimore, MD 21204

* Author to whom correspondence should be addressed.

[⊗] Abstract published in *Advance ACS Abstracts,* April, 1, 1997.

(1) HNIW is the acronym for hexanitrohexaazaisowurzitane, 2,4,6,8,10,12-hexanitrohexaazatetracyclo[5.5.0^{5,9}.0^{3,11}]dodecane.

(2) Toscano, J. P. Ph.D. Thesis, Yale University, 1993.

(3) Results of the unpublished X-ray structure determination were kindly supplied by Dr. Richard Gilardi, Naval Research Laboratory, Washington, DC.

(4) Pace, M. D. *J. Phys. Chem.* **1991**, *95*, 5858−5864.

(5) We follow the convention that *J* (not 2*J*) is the electrostatic contribution to the S−T gap, and that positive *J* corresponds to a triplet ground state (ferromagnetic coupling).

(6) Paddon-Row, M. N. *Acc. Chem. Res.* **1994**, *27*, 18−25 and references therein.

(7) Rajca, A. *Chem. Rev.* **1994**, *94*, 871−893.

(8) Eaton, G. R.; Eaton, S. S. *Acc. Chem. Res.* **1988** and references therein.

(9) For some recent references see: Curtiss, L. A.; Naleway, C. A.; Miller, J. R. *J. Phys. Chem.* **1995**, *99*, 1182.

S0002-7863(96)03161-7 CCC: $14.00

magnetic resonance spectra, an averaged value is obtained with no clear relationship to a specific radical−radical distance.[10]

Radical pairs created by homolysis in single crystals present an opportunity to observe electron−electron exchange for well-characterized structures without chains of bonds connecting the radical centers. In many radical pairs *J* is inaccessible because it is small compared to *kT*, but large compared to magnetic interactions.[11] Under these conditions EPR spectra are insensitive to the magnitude and sign of *J*, and can usually be interpreted in terms of Zeeman, zfs, and nuclear hyperfine splitting (hfs) alone.[12] It has, however, been possible to measure *J* in several radical pairs, including alkyl radicals in urea channels (using EPR splittings)[13] and carbon-centered radicals either in single crystals of diacyl peroxides (using EPR splittings)[14] or in X-irradiated 1-methyluracil (using accidental degeneracy of S_0 and T_{-1} in the applied field).[15]

As shown below, $^{15}NO_2/^{15}NO_2$ pairs in α-HNIW provide an unusually clear example of long-range exchange coupling, because their nuclear spin system is very simple and their structure is well-defined, although using the results to test theory may be difficult until the structure of the nonbonded material between the radicals is determined.

Experimental Section

CAUTION: Although HNIW is not a primary explosive, it is a powerful one and should be treated with extreme care. Crystals used in this work weighed less than 2 mg.

Methods, instrumentation, and materials used in EPR spectroscopy, as well as isotope exchange and crystal growth, have been described elsewhere.[16] HNIW-^{15}N contained 86% ^{15}N in its six nitro groups.

Results

Nature and Stability of Radical Intermediates. EPR spectra recorded after photolysis of α-HNIW-^{15}N single crystals at 15 K, but before warming, included prominent signals with large *g* anisotropy and anisotropic doublet splittings as large as 400 G. In photolyzed crystals of nitramines, large *g* anisotropy is due to incompletely quenched orbital angular momentum of NO, and large doublet splitting is due to electron−electron dipolar interaction within closely spaced radical pairs. These signals were thus attributed to two radical pairs containing NO, but they proved difficult to analyze in detail because of excessive line width. They were irreversibly destroyed by warming to 80 K and will not be discussed further.

Of the original paramagnetic material about half survived warming to 80 K. It also survived further annealing at 195 K,[17] to give the spectra shown in Figure 1. These spectra, like all spectra discussed below, were measured at 80 K, where peaks of the small amounts of species that involve NO are too broad to observe.

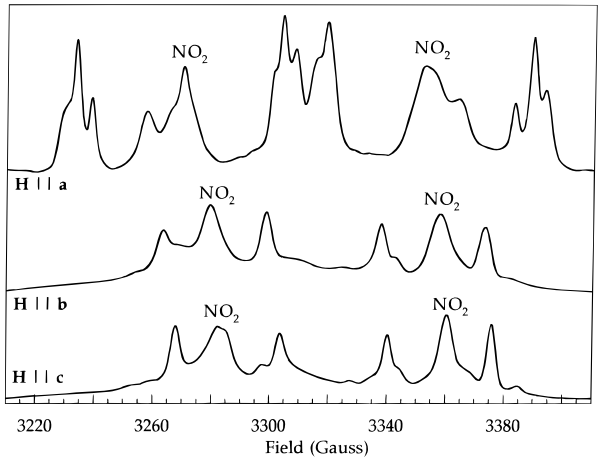

Figure 1. EPR spectra at 80 K from single α-HNIW-^{15}N crystals after photolysis for 60 min at 20 K and annealing for 30 min at 195 K. Doublets for isolated cavity $^{15}NO_2$ are labeled; other peaks are satellites due to pairs A−C. Spectra with the field along *b*- and *c*-axes were measured in a single experiment.

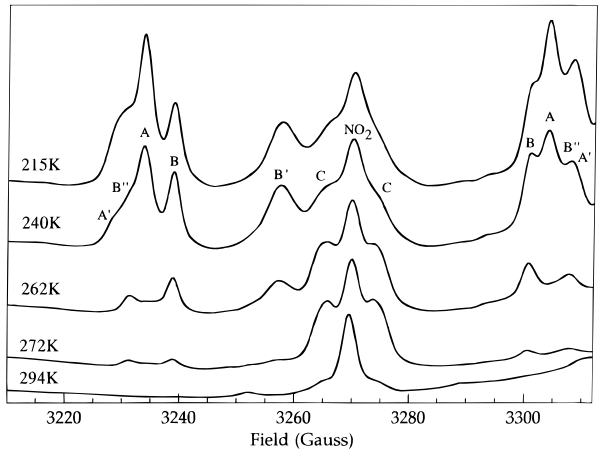

Figure 2. EPR spectra at 80 K from a single α-HNIW-^{15}N crystal (H||*a*) after photolysis for 60 min at 20 K and sequential annealing to the indicated temperature. Only the low-field half of each spectrum is shown. Labels are explained in the text.

The patterns of Figure 1 are dominated by an ^{15}N doublet splitting of 75 to 85 G, which separates the spectra into high-field and low-field halves. In an unlabeled crystal ^{14}N hfs gives a corresponding triplet of patterns that overlap because of the smaller nuclear splitting constant.

Four species contribute to the spectra of Figure 1. Three of them can be successively destroyed by stepwise annealing between 215 and 294 K, as shown in Figure 2, which corresponds to the low-field half of the top spectrum in Figure 1. As explained below, the three species that decay are NO_2/NO_2 radical pairs (A−C), and the one that survives is isolated cavity NO_2, studied first by Toscano[2] and subsequently by Pace.[4] Peaks due to the three radical pairs are labeled accordingly in Figure 2 and appear as satellites of the absorption for isolated cavity NO_2.

Spectral integration showed that, of the paramagnetic material that survived warming from 80 to 190 K, the fractions of pair A, pair B, pair C, and isolated NO_2 were approximately 51%, 33%, 11%, and 5%, respectively. Pair A decays within a few minutes at 240 K, pair B at 260 K, and Pair C at 290 K.

(10) Zimmt, M. B.; Doubleday, C.; Turro, N. J. *J. Am. Chem. Soc.* **1984**, *106*, 3363. Closs, G. L.; Forbes, M. D. E.; Norris, J. R. *J. Phys. Chem.* **1987**, *91*, 3592.

(11) At 10 K, *kT* is about 20 cal/mol. The largest magnetic energy is typically the Zeeman splitting of 1 cal/mol at X-band, and more relevant magnetic interactions, such as zfs and hfs, are 10−1000 times smaller. When the ground state is a triplet, EPR intensities are insensitive to the magnitude of large *J* values.

(12) (a) Weltner, W. *Magnetic Atoms and Molecules*, 2nd ed.; Dover Publications Inc.: New York, 1989; Chapter III. (b) Wertz, J. E.; Bolton, J. R. *Electron Spin Resonance*, 2nd ed.; Chapman and Hall: New York, 1986; Chapter 10.

(13) (a) Griller, D.; Casal, H. L.; Hartstock, F. W.; Kolt, R.; Park, J. M.; Wayner, D. D. M.; Northcott, D. J. *J. Phys. Chem.* **1987**, *91*, 2235. (b) Griller, D.; Casal, H. L.; Hartstock, F. W.; Kolt, R.; Park, J. M.; Wayner, D. D. M.; Northcott, D. J. *J. Phys. Chem.* **1987**, *93*, 1666.

(14) Feng, X. W. Thesis, Yale University, 1991.

(15) Flosmann, W.; Westhof, E.; Mueller, A. *Phys. Rev. Lett.* **1975**, *34*, 959.

(16) Ryzhkov, L. R.; McBride, J. M. *J. Phys. Chem.* **1996**, *100*, 163.

(17) Warming from 80 to 195 K simplified the spectra slightly by removing traces of material with slightly larger splitting than pairs A−C discussed below. This might represent very small amounts of ***ab*** or ***a′b*** pairs, see Discussion.

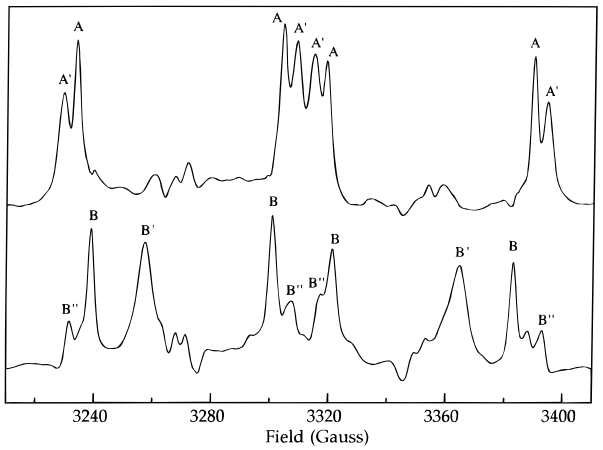

Figure 3. EPR spectra of radical pairs A (top trace) and B (bottom trace) obtained by difference from the spectra of Figure 2. For example, the top spectrum is the 215 K spectrum minus 110% of the 240 K spectrum.

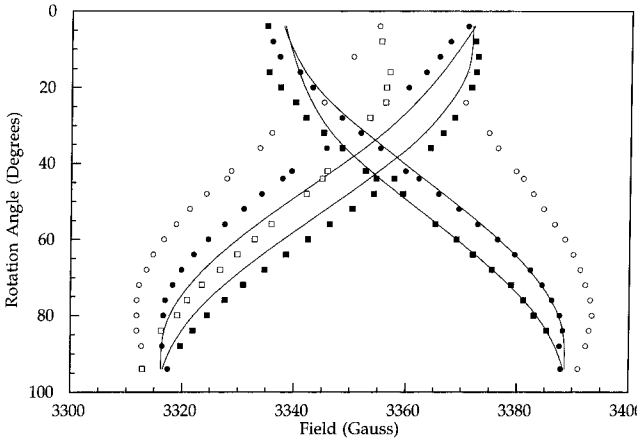

Figure 4. Variation in high-field pair A peak positions during crystal rotation with H in the *ab* plane. Circles and squares differentiate observed peaks due to symmetry-related but magnetically-independent orientations. Filled symbols denote *J*-independent "zfs" or A peaks, while open symbols denote "*J*" or A′ peaks. Solid curves show calculated positions for zfs peaks with use of average *g*, zfs, and hyperfine tensors as described in the text. For this crystal mounting rotation angles range from 5° (*b*-axis) to 95° (*a*-axis).

Integration confirmed the visual impression that each radical pair decays to diamagnetic products, forming neither one of the other pairs nor cavity NO_2.[18] The modest increase in the amplitude of the C lines after warming to 262 K results only from decreased line width.

Differences between appropriately scaled *a*-axis spectra provided the spectra of pairs A and B shown in Figure 3. Peaks that are significant in the subsequent analysis are labeled. Other small peaks are probably artifacts of subtraction. The analogous *a*-axis spectrum of pair C showed only a closely spaced pair of lines flanking each hyperfine line of cavity NO_2.[19]

ZFS, hfs, and *g*-Tensors of the Radical Pairs. Figure 4 plots peak positions in the high-field half of the spectrum for pair A as the crystal is rotated about the *c*-axis. At the rotation extremes, where the magnetic field lies along an orthorhombic axis, all four symmetry-related orientations of any given species are magnetically equivalent, and a single set of four lines appears

(18) Less that 4% of any decaying signal intensity reappears in a surviving signal.

(19) Experimental, differences, and simulated *a*- and *b*-axis spectra for pairs B and C are available in the Supporting Information as Figures 2s−5s.

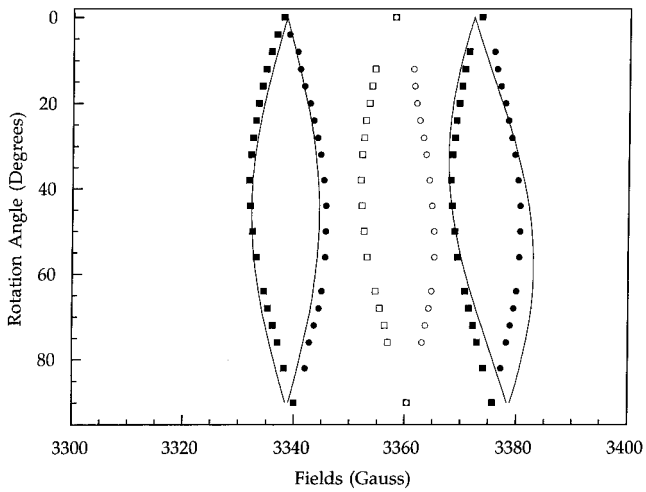

Figure 5. Analogue of Figure 4 for crystal rotation with H in the *bc* plane from 0° (*b*-axis) to 90° (*c*-axis).

in the high-field half of the pair A spectrum. Filled symbols denote the two sharper peaks labeled A in Figure 3, and open symbols denote the two broader peaks labeled A′. For other field directions in the *ab* plane the four symmetry-related orientations separate into two sets of two magnetically equivalent orientations, and each of the four lines splits into two, one from each set. The four lines due to one set are denoted by circles and those due to the other set by squares.[20] Figure 5 is an analogous plot for crystal rotation about the *a*-axis from *b* to *c*.

Figure 5 shows that the splitting of the sharp satellites labeled A is nearly constant (35−36 G) for all magnetic field directions in the *bc* plane. Figure 4 shows that for fields in the *ab* plane the splitting changes sign and becomes about twice as large (−70 G) along *a* as along *b*. This behavior is expected for the axially-symmetric, traceless zfs tensor that would arise from magnetic dipole interaction between two radicals separated by a vector parallel to the *a*-axis. Signs were assigned to the splittings accordingly.

A preliminary analysis can be carried out neglecting the primed peaks and assuming that the four A peaks of pair A represent a double doublet with a large splitting due to hfs of one ^{15}N and a smaller splitting due to zfs of the radical pair. Of course both ^{15}N nuclei of an $^{15}NO_2/^{15}NO_2$ radical pair should contribute hfs, but, as explained below, approximate analysis assuming splitting by a single ^{15}N with an average coupling constant is appropriate for the sharp peaks. The remainder of this paper will refer to the sharp, unprimed satellites as "zfs" lines and the broader primed or doubly primed peaks as "*J*" lines.

In this analysis of the four zfs lines, zfs and hfs were both approximated as first-order perturbations to the Zeeman energy. Thus an average *g* tensor was fit to the average of the four line positions, an average ^{15}N hfs tensor was fit to the difference between the average of the high-field line positions and the average of the low-field line positions, and a zfs tensor was fit to the average of the splitting in the high-field doublet and the splitting in the low-field doublet. Table 1 presents the resulting tensors, and the solid lines in Figures 4 and 5 show how well this simple model fits the observed position of the zfs lines.[21] Since high precision is not necessary for interpreting the results, it was not judged worthwhile to conduct a full-scale non-perturbational treatment.

(20) A′ peaks that would be denoted by open squares at high field are obscured by the A peaks and are omitted from Figure 4.

(21) Crystal orientations, line positions, and output of the refinement programs are available in the Supporting Information.

Table 1. *g*,[a] ^{15}N hfs,[b] and *ZFS* Tensors[c] of Pair A

tensor element	g_{xx}	g_{yy}	g_{zz}	A_{xx}	A_{yy}	A_{zz}
eigenvalue	2.0105(1)	1.9953(1)	2.0044(1)	−78.9(3)	−66.9(4)	−85.4(4)
eigenvector[d]	0.7236	0.0115	0.6902	−0.2342	0.0260	0.9718
	−0.5524	0.6092	0.5690	0.7709	0.6140	0.1694
	0.4139	0.7929	−0.4471	−0.5923	0.7889	−0.1638
angular error, deg	0.6	0.7	0.5	1.7	1.7	1.0[o]
tensor element	$3D_{xx}$	$3D_{yy}$	$3D_{zz}$	A'_{xx}	A'_{yy}	A'_{zz}
eigenvalue	40.2(2)	33.1(2)	−73.1(2)	−69.0	−63.2	−93.5
eigenvector	0.0074	−0.0007	0.9999	0.2893	−0.2378	0.9272
	0.1922	0.9813	−0.0021	0.9541	−0.0064	−0.2993
	0.9813	−0.1922	−0.0071	0.0771	0.9713	0.2251
angular error, deg	2.5	2.5	0.3	*e*	*e*	*e*

[a] The **g** tensor was refined with use of four crystal mountings and 195 orientations (rms deviation 0.0004). [b] The hfs tensor (Gauss) was refined with use of four crystal mountings and 160 orientations (rms deviation 1.1). [c] The zfs tensor (reported as line separations in Gauss) was refined with use of four crystal mountings and 190 orientations (rms deviation 2.1). [d] Eigenvector direction cosines relative to the *a*, *b*, and *c* crystallographic axes. [e] Errors in the *A*′ eigenvalues and in the A'_{zz} direction should be about twice as large as those for the **A** tensor. Directions of A'_{xx} and A'_{yy} are unreliable because of near-degeneracy.

The zfs tensor for pair A in Table 1 is nearly axially symmetric, and the large negative eigenvector, corresponding to the vector connecting the radicals, lies within 0.5° of the *a*-axis. Using the point dipole approximation the distance between the radicals is estimated to be 9.26 Å. This is close to the crystallographic *a*-translation of 9.485 Å that relates the centers of neighboring solvent cavities.

The averaged *g* and ^{15}N-hfs tensors for pair A are similar enough to the tensors for NO_2 isolated in solvent cavities of α-HNIW to confirm the interpretation that pair A consists of two NO_2 molecules in adjacent cavities, but there are significant differences. Toscano's *g* tensor[3] for isolated cavity NO_2 is consistent with the literature[22] in showing a low-*g* eigenvector (g_{yy} = 1.992) aligned with the molecular O−O vector, an intermediate-*g* eigenvector (g_{zz} = 2.002) parallel to the molecular C_{2v} axis, and a high-*g* eigenvector (g_{xx} = 2.006) normal to the O−N−O plane. The *g*-tensor eigenvectors of Table 1 are parallel to the corresponding eigenvectors for cavity NO_2 within 6°, although the eigenvalues are uniformly slightly larger.[23]

The average g_{yy} and A_{yy} eigenvectors in Table 1, corresponding to the O−O axis of the NO_2 molecules, are parallel to one another within 0.9°. A_{yy} is parallel to the corresponding eigenvector of cavity NO_2 within 6.8°, and after correcting for the magnetogyric ratio of ^{15}N, the A_{yy} eigenvalues agree within 1.7 G (3%). All of these observations suggest that the O−O vectors of the two NO_2 radicals in pair A are parallel to one another and to that of isolated cavity NO_2.

Despite the good agreement between the A_{yy} eigenvectors of pair A and isolated cavity NO_2, there is a pronounced discrepancy for the A_{xx} and A_{zz} eigenvectors. Not only do these eigenvectors of pair A diverge from the corresponding eigenvectors of isolated cavity NO_2 by about 43° (and from their own *g* eigenvectors by 37°), but also the A_{xx} and A_{zz} eigenvalues differ from one another by only 6.3 G, 24% of the difference for isolated cavity NO_2. These differences may be explained by assuming that the A_{xx} and A_{zz} eigenvectors are averages for two NO_2 molecules that have parallel O−O vectors but different phases of rotation about this vector. Averaging of the corresponding *g* eigenvectors is less significant because of small anisotropy.

While the accuracy of the data and the fitting procedure does not support precise determination of the phase of rotation of the two NO_2 molecules of pair A, two approximations give similar qualitative results. One approach is to find the amount of relative rotation required to reduce $A_{xx} - A_{zz}$ by 76%. This angle is 62°, meaning that the C_{2v} axes of the two molecules are rotated plus and minus 31° from their average, so that one of the two is within about 10° of the orientation of isolated cavity NO_2.

The second approach is to assume that one of the NO_2s has the same hfs tensor as isolated cavity NO_2 and to find the other tensor that must be averaged with it to give the observed tensor. This difference tensor is presented in Table 1 as *A*′ eigenvalues and eigenvectors. The *A*′ eigenvalues are reasonable in magnitude and symmetry for an isolated NO_2 radical. The well-determined A_{zz} eigenvector (C_{2v} axis) is within about 10° of the direction inferred from the first approach.

It thus appears that the signals described above are due to a pair of weakly interacting NO_2 molecules occupying solvent cavities related by the *a*-axis translation of the α-HNIW unit cell, and that one of these molecules is oriented the same as isolated cavity NO_2 within about 10°, while the other is rotated by some 60−75° about the O−O vector.

A likely cause of the discrepancy between calculated lines and observed points in Figure 4 is that the simulation routine required identical *g* and hfs tensors for the two radicals, rather that assigning each its individual tensor.

Lack of good data made it more difficult to determine corresponding tensors for pair B and impossible for pair C. When crystals containing both species were rotated, the lines of pair B tracked those of pair A, but showed reduced zfs splitting. Thus it was assumed that the zfs tensor of pair B, like that of pair A, is axially symmetric about the *a*-axis. The spectrum of Figure 3 was then used to estimate a maximum zfs splitting of 62 G corresponding to 9.67-Å separation. The *g* and hfs tensors of pair B are likely similar to those of pair A, but were not refined.

The zfs splitting of pair C is so small that it could be estimated only by applying the magnetic field along the orthorhombic axes to reduce the complexity caused by overlapping patterns. The zfs splitting along the *a*-axis was 8 G, while that along the *b*-axis appeared to be about twice as large, as expected for a radical−radical separation of ∼13 Å along the 13.23-Å crystallographic *b*-axis.

***J* Coupling of the Radical Pairs.** The preliminary analysis above ignores the primed (*J*) lines in the spectra and assumes splitting by a single ^{15}N with the hfsc of an isolated radical, rather than splitting by both radicals with halved coupling constants as is observed in tightly coupled radical pairs. This approach may be justified by considering the influence of small exchange couplings on radical pair spectra.

(22) Weltner, W. *Magnetic Atoms and Molecules*, 2nd ed.; Dover Publications Inc.: New York, 1989; Chapter II, pp 104−108.

(23) The source of these **g** shifts is unclear. ZFS is far too small to shift the average line position.

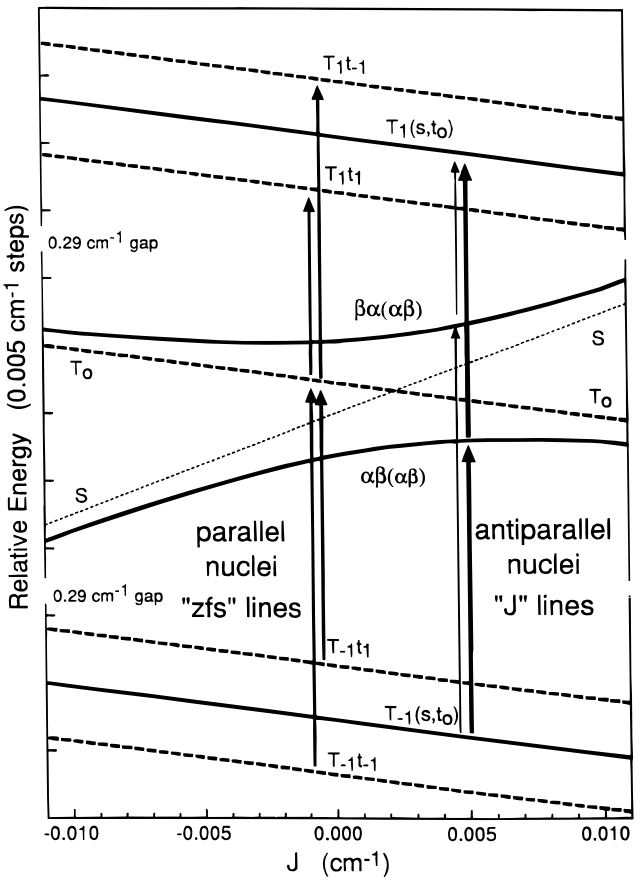

Figure 6. Calculated energy levels for the magnetic eigenstates of pair A in a field parallel to the *a*-axis as a function of assumed exchange coupling. Dashed lines denote states with parallel nuclei. Solid lines, denoting states with antiparallel nuclei, have an avoided crossing that gives strong *J*-lines (heavy arrows) and weak ones (light arrows). The line whose center is $\alpha\beta(\alpha\beta)$ also holds for $\beta\alpha(\beta\alpha)$, as well as $\beta\alpha(\alpha\beta)$ for $\alpha\beta(\beta\alpha)$. Note that the vertical scale has breaks, and that T_o is closer to T_1 than to T_{-1} because of zfs.

Although the $\alpha\alpha$ (T_1) and $\beta\beta$ (T_{-1}) electronic spin functions are high-field eigenstates for typical radical pairs for any value of *J*, the $\alpha\beta + \beta\alpha$ (T_o) and $\alpha\beta - \beta\alpha$ (S) states are more problematic. T_o and S are eigenfunctions of $S_1 \cdot D \cdot S_2$, the electron−electron dipolar coupling, and of $JS_1 \cdot S_2$, the electrostatic energy difference between singlet and triplet, but they can be mixed toward $\alpha\beta$ and $\beta\alpha$ by magnetic differences between the two radicals, such as different *g* values or nuclear states. Such mixing is important only when the magnetic difference between the radicals is significant compared to the sum of $S_1 \cdot D \cdot S_2$ and $JS_1 \cdot S_2$.

Figure 6 presents energy levels for pair A, with varying assumed values of *J*, as determined by diagonalizing the 16 × 16 matrix of Hamiltonian 1 for two electrons and two ^{15}N nuclei.

$$H = \beta \mathrm{H} g_1 \mathrm{S}_1 + \beta \mathrm{H} g_2 \mathrm{S}_2 + \mathrm{S}_1 D \mathrm{S}_2 + \mathrm{I}_1 A_1 \mathrm{S}_1 + \mathrm{I}_2 A_2 \mathrm{S}_2 - J\mathrm{S}_1 \cdot \mathrm{S}_2 \quad (1)$$

The matrix elements were constructed using the formulas of Pilbrow and Smith,[24] which require identical hfs and *g* tensors for the two radicals and point-dipole zfs. The averaged hfs and *g* tensors determined above were used, and the zfs tensor was calculated for point dipoles separated by 9.26 Å along the *a*-axis, in accord with the experimental zfs tensor. A magnetic field of 3300 G was applied along the *a*-axis. Note that because of zfs, the S and T_o states cross at $J = 0.0023$ cm^{-1}, rather than at $J = 0$.

The dashed lines in Figure 6 show the t_1 and t_{-1} nuclear states, for which there is no $S-T_o$ mixing because the radicals are magnetically equivalent.[25] Because the zfs lines, which arise from transitions involving these nuclear states, are independent of *J*, they could be used above to determine *g*, hfs, and zfs tensors.

The solid lines in Figure 6 show states in which the two radicals have opposite nuclear spins.[26] For these states there is an avoided crossing of S and T_o that segregates the electron spins and influences the frequency and intensity of the *J* lines.

In Figure 6 consider the "T_{-1}" transitions that originate from T_{-1} electronic levels and the "T_1" transitions that terminate in T_1 levels. In a fixed-frequency spectrometer the T_{-1} zfs lines, the first and third A lines in Figure 3, occur at lower field than the corresponding T_1 zfs lines (second and fourth). Under the conditions of the figure, $J = 0.003$ cm^{-1} will give two T_{-1} *J* lines. They are the first and third A′ lines in Figure 3. The stronger T_{-1} *J* line (the third A′ line) is stronger than the T_{-1} zfs lines and occurs at a higher field (lower frequency) than their average. Similarly the stronger of the T_1 *J* lines (the second A′ line) is stronger than the T_1 zfs lines and occurs at a lower field than their average. As *J* increases, the weaker *J* lines would disappear and the stronger *J* lines would strengthen, because of nuclear degeneracy, to twice the intensity of the corresponding zfs lines and approach the average of their frequencies, that is, the EPR spectrum would approach the pair of 1:2:1 hfs patterns expected for a triplet pair.

The sign of *J* relative to that of zfs is directly displayed by the shift of the stronger *J* lines relative to the average of the flanking zfs lines. The stronger *J* lines involve the $S-T_o$ mixture that lies closer to T_o. As shown in Figure 6, they involve the lower branch for positive *J* and would involve the upper branch for negative *J*. The stronger T_{-1} *J* line will always fall between the two T_{-1} zfs lines, lying to high field of their average if *J* is positive and vice versa. The shift is opposite for the T_1 lines. In Figure 7 pair A is oriented so that the first and third zfs lines involve T_{-1}, and in Figure 8 the second and fourth. In both cases the strong *J* line between the two T_{-1} zfs lines is shifted to high field from their average (and vice versa for the T_1 lines) demonstrating that *J* is positive. The strong *J* lines of pair B, whose zfs lines are almost identical to those of pair A, shift in the opposite direction, establishing a negative value for *J* (see peaks B′ of Figure 3, and Figure 2s in the Supporting Information).

For pair A the positions and intensities of the *J* lines are sensitive to the magnitude of *J*. Both the *a*- and *b*-axis spectra are well described by $J = +0.003(1)$ cm^{-1}, as shown by Figures 7 and 8, where each resonant field was determined by iterative diagonalization as in ref 24.[27]

For pair B, a *J* of -0.007 cm^{-1} gives a qualitatively reasonable fit to the *a*-axis spectrum, but is inconsistent with the *b*-axis

(24) Pilbrow, J. R.; Smith, T. D. *Coord. Chem. Rev.* **1974**, *13*, 173.

(25) The assumption of equivalent hfs and **g** tensors obscures the influence of mixing due to differences in orientation of the two NO_2s. The effect should be small, because the *y* axes are parallel and the *xx*−*zz* anisotropy of the tensors is modest. At its largest the off-diagonal matrix element favoring $S-T_o$ mixing for the t_1 and t_{-1} nuclear states would be about an order of magnitude smaller than for the $\alpha\beta$ and $\beta\alpha$ nuclear states, and usually it would be much smaller still. The approximation may contribute to the difference between observed and calculated line positions in Figures 4 and 5.

(26) Each solid line corresponds to two states whose energies are not affected by taking antisymmetrized combinations.

(27) The same value of *J* was used to give a qualitatively satisfactory simulation of the position and intensity of the *J* lines of one of the asymmetric units plotted in Figure 4 for all phases of rotation. See Figure 1s in the Supporting Information.

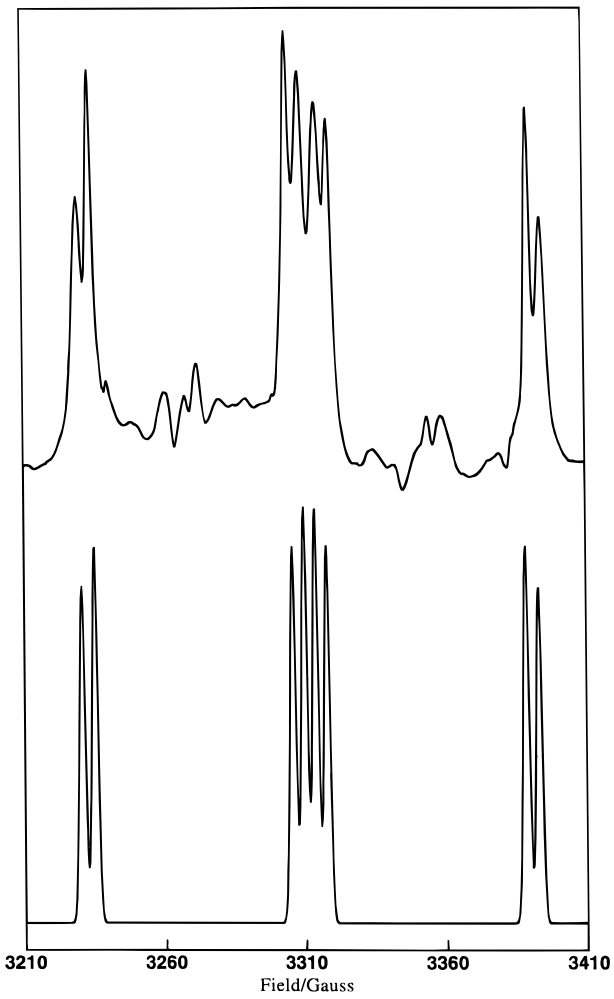

Figure 7. Experimental (top) and calculated (bottom) *a*-axis spectra for pair A. The calculated spectrum assumes the experimental averaged *g* and hfs tensors, a *J* coupling of 0.003 cm^{-1}, and a zfs tensor for point dipoles separated by 9.24 Å along the *a*-axis (the lattice spacing is 9.485 Å).

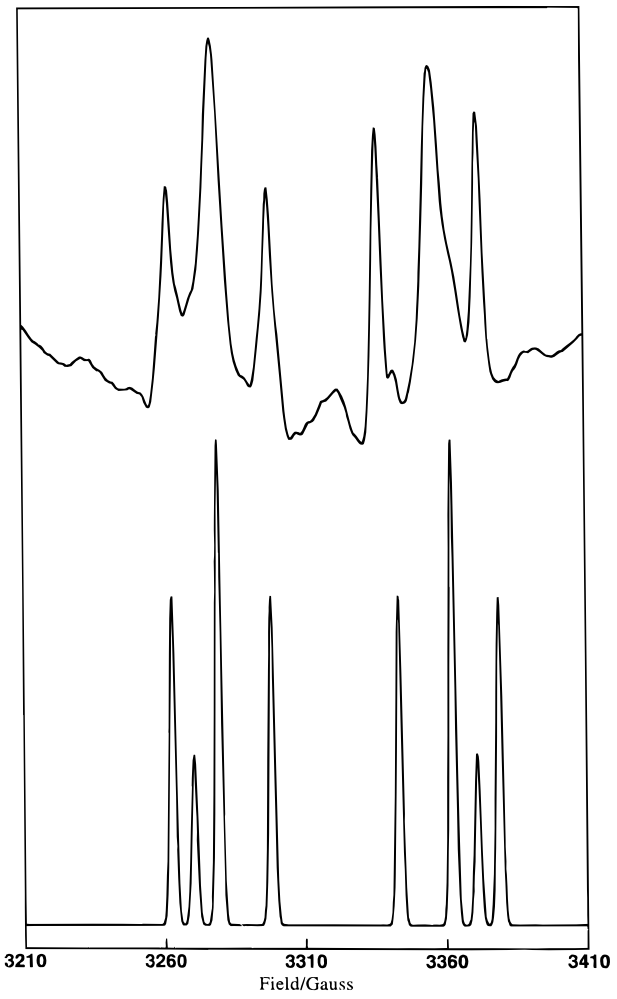

Figure 8. Experimental and calculated *b*-axis spectra of pair A. The calculated spectrum was based on the same assumptions as in Figure 7.

spectrum.[28] The only way we have found to fit both spectra is to assume the presence of two populations with the same zfs and hfs tensors. The major population would have $J = -0.004$ cm^{-1}, and the minor population would have $J = +0.0033$ cm^{-1}. Their *J* peaks are labeled B′ and B″, respectively, in Figure 3.

For pair C the spectrum is much less well defined, but like pair B it can be accommodated by assuming two different values of *J*, 0.000 and $+0.003$ cm^{-1}.[28]

Discussion

The results of this study bear on two questions that are of general interest in organic solid-state chemistry. The first question concerns the ease and specificity of short-range translational motion of small molecules in a molecular crystal. Defect mobility in energetic materials, such as HNIW, may influence whether trace amounts of decomposition during storage result in a permanent change in sensitivity to shock or other modes of initiation. The second question concerns the nature of intermolecular exchange coupling in radical pairs of well-defined structure.

Translational mobility. Previous inferences about the translational mobility of NO and NO_2 radicals in damaged α-HNIW crystals were of two kinds. EPR signals due to radicals isolated in clathrate cavities survived for years at room temperature and even when the crystals were heated to 85 °C for 14 h in vacuum.[3] This showed that long-range translation by hopping from cavity to cavity is strongly inhibited.

At the same time some mobility is necessary to convert precursor molecules into the isolated radicals, whose signals grew when a photolyzed crystal was subsequently annealed overnight at room temperature. It was provisionally assumed that significant amounts of NO and NO_2 had been preformed by low-temperature photolysis, but that they migrated only short distances and were undetected by EPR because of excessive line width caused by occupying a wide variety of interstitial sites.[29] At room temperature the translational mobility of interstitial molecules might become sufficient to allow them to migrate much further and find rare clathrate sites that contain no water of solvation, where they could be tightly trapped and uniformly ordered to give sharp signals.

The present observations on radical pairs A−C suggest less mobility. When they are formed by photolysis at very low temperature, the NO_2 pairs seem already to be tightly trapped in immediately adjacent cavities. In pair A, where the NO_2 orientation can be determined, it is closely similar to that of the isolated species. This suggests that it is not necessary for the isolated NO_2 to diffuse a substantial distance and find vacant

(28) Figures 2s−5s in the Supporting Information present observed and simulated *a*- and *b*-axis spectra for pairs B and C.

(29) Such line width is implausible for isolated NO_2, whose signal is less anisotropic than that of NO, but it is conceivable that the signal was broadened by zfs anisotropy due to the existence of NO_2 in a variety of radical pairs.

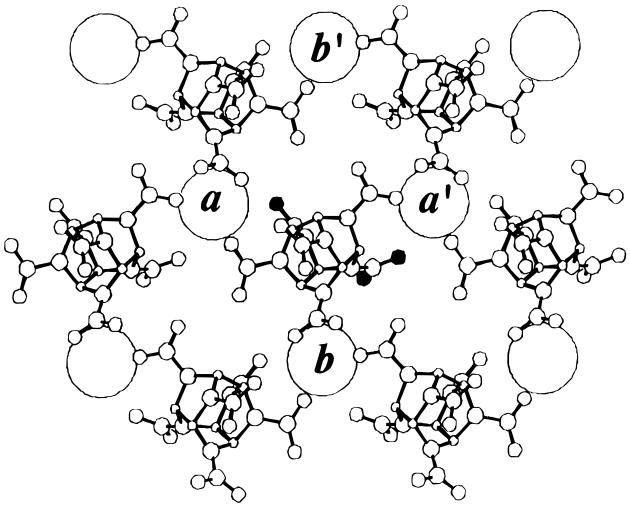

Figure 9. View along the *c*-axis showing a layer of α-HNIW and the adjacent water cavities. The smallest spheres denote carbon, and hydrogens are omitted. For the central molecule, the darkened oxygens in the two nitro groups furthest from the viewer are closest to the three cavities (***a***, 2.74 Å, ***a′***, 2.94 Å; ***b***, 3.88 Å). In pairs A and B, NO_2 molecules occupy cavities ***a*** and ***a′***; in pair C they occupy ***b*** and ***b′***.

cavities in order to give a sharp spectrum. Translational mobility of NO_2 in the pairs is remarkably low, since they survive almost to 0 °C without making even one jump to a neighboring cavity, and they ultimately decay by collapse to diamagnetic products, not by separation to give isolated NO_2.

The signal of isolated NO_2 begins to grow only long after the pairs have disappeared, doubling in intensity after 12−18 h at room temperature. It is possible that the pairs collapse to a dimer that redissociates at higher temperature. Alternatively the isolated NO_2 may derive from other intermediates, ones that are invisible to EPR because they are diamagnetic molecules or singlet radical pairs. Although EPR allows study at very low conversion, where the crystal lattice remains intact and structures are well defined, such low conversion is difficult to measure independently, so it is hard to be certain that the species observed by EPR dominate the reaction pathway.

In any case, the present results suggest that isolated NO and NO_2 need not have moved far enough to find vacant cavities. Thus the diffusion that separates the radicals might be limited to a few hops, which might suffice to reduce a driving force that is due to overlapping of the two single-particle strain fields in the lattice. With such low mobility, free radicals and mechanical strain might accumulate during storage of this kind of material and alter its sensitivity.

Translational Specificity. Whether or not pairs A−C are on dominant decomposition pathways, they reveal striking specificity in the motion of reaction fragments. As shown in Figure 9, each nitramine molecule in α-HNIW is adjacent to three symmetry-related solvent cavities. The central molecule touches ***a***, ***a′***, and ***b***. Cavities ***a*** and ***a′*** are related to one another by translation along *a* and to ***b*** (and ***b′***) by *b*-glide planes.

One might expect that decomposition of the central molecule in Figure 9 could generate three pairs of cavity-trapped NO_2 radicals, occupying ***aa′***, ***ab***, or ***a′b***.[30] Of these only ***aa′*** is observed, and it occurs in two noninterconverting forms, pair A and pair B, which differ in separation by 0.41 Å, presumably because of different arrangements of other reaction fragments in the space between the cavities. If ***ab*** and ***a′b*** are formed in large amount,[17] either they must decay rapidly by 20 K, while ***aa′*** survives to 240−260 K, or they must possess such strong antiferromagnetic coupling that the triplet state is not populated at 80 K. Neither of these conditions seems likely.

Even more remarkable is the specificity involved in forming pair C, where the NO_2 radicals occupy ***b*** and ***b′***. It is not obvious how an NO_2 makes its way to ***b′*** through a barrier of nitramine molecules, where space-filling models show no obvious opening, nor why neither ***ab′*** nor ***a′b′*** is observed. Strong anisotropic reaction-generated stress must be involved in generating ***bb′***.

One plausible decomposition mechanism for forming an NO_2 radical pair requires nitramine groups separated by two carbons. Concerted or stepwise cleavage of three bonds in the $O_2N-N-C-C-N-NO_2$ substructure could generate the radical pair and leave two imine groups in a tricyclic byproduct, $O_2N\cdot\ N{=}C\ \ C{=}N\ \cdot NO_2$. Of the 15 possible pairs among the six nitramine groups of HNIW, 11 possess the required substructure.[31] The two NO_2 groups closest to ***a*** and ***a′***, however, do not. Thus, if this fragmentation occurs, the NO_2s that move into the cavities are not their nearest neighbors. Unfortunately spectral complexity makes a test with selective ^{15}N labeling impractical.[16]

Exchange Coupling. Although the use of *J* lines to measure exchange interactions is hardly new,[32] the present system provides unusually clean examples of covalently independent molecular radicals with known, fixed separation and orientation. Labeling with ^{15}N was crucial in simplifying the EPR spectrum to give four zfs transitions, which define the pair structure and are insensitive to *J*, and four *J* transitions, whose position and intensity is very sensitive to the magnitude and sign of *J*.

The most complete analysis was for pair A, where spectra for a large number of field directions were checked by simulation. Despite small discrepancies attributable to approximations in the simulation algorithm, it is clear that the NO_2s in pair A are 9.26 Å apart and coupled by 0.003(1) cm^{-1} (0.009 cal/mol) ferromagnetically (triplet below singlet).

Although this exchange coupling is small, it is certainly much larger than through-space interaction at such distances.[33] Pair A could be used to test theoretical methods of estimating *J* for non-covalent pairs in condensed media, particularly if one could reliably determine the nature and orientation of the other molecules that are packed between the distant radicals and enable them to communicate.

Pair B underlines the subtlety of coupling through intervening molecules. In two canonical directions of the magnetic field pair B gives the expected four zfs transitions but seems to show at least six, rather than the expected four, *J* transitions. Superposition of two calculated spectra for a single pair geometry with *J* values of +0.0033 and −0.004 cm^{-1} gives a plausible match to the spectra observed for both field directions. The sharpness of the zfs lines that are shared by these two versions of pair B shows that they do not differ in radical separation by as much as 0.3 Å and that orientation of the individual radicals does not vary enough to alter the observed hfs. Despite the structural similarity their *J* values differ in sign as well as magnitude.

(30) The centers of the ***a*** and ***a′*** cavities are closer to nitramine oxygens of the central molecule (2.74 and 2.94 Å, respectively) than is the center of the ***b*** cavity (3.88 Å), but it is not obvious which NO_2 groups should be lost in the decomposition.[16] Center-to-center distances of the cavities are 9.49 Å for ***aa′*** and 8.14 Å for ***ab*** and ***a′b***.

(31) Some pairs have unfavorable conformations for concerted fragmentation.

(32) Glarum, S. H.; Marshall, J. H. *J. Chem. Phys.* **1967**, *47*, 1374.

(33) Analogous one-electron coupling is several orders of magnitude smaller through-space than through intervening alkane molecules. Curtiss, L. A.; Naleway, C. A.; Miller, J. R. *J. Phys. Chem.* **1993**, *97*, 4050.

Perhaps the two versions of pair B have almost identically arranged NO_2 radicals, but there is a difference in the packing of other molecules between them that alters the coupling mechanism. That the two versions decay at the same rate and are always observed in the same ratio may suggest that they equilibrate.

Pair C also gives spectra that are most easily explained by a single pair structure with two different *J* values, but the spectra are of lower quality.

The five *J* values are considerably smaller than those for some organic and organometallic diradicals of comparable separation that are connected by a chain of covalent and coordinate bonds, but not much smaller than those for some transition metal complexes with paramagnetic ligands.[8,34] Their magnitude may be useful in prediction and empirical evaluation of long-range *J* coupling in other systems.

Acknowledgment. This work was supported by Grant No. N00014-90-J-4015 from the Mechanics Division of the Office of Naval Research. We are grateful for ideas, materials, and experimental assistance to Drs. Michael C. Biewer, John P. Toscano, John R. Miller, Richard S. Miller, Richard Gilardi, and William Koppes and Professor Gary Brudvig.

Supporting Information Available: Plot of calculated zfs- and *J*-line positions of pair A, experimental and simulated spectra of pairs B and C, and tabulated experimental data for from crystal mountings used to determine the **g**, hfs, and zfs tensors of pair A (22 pages). See any current masthead page for ordering and Internet access instructions.

JA9631615

(34) Damoder, R.; More, K. M.; Eaton, G. R.; Eaton, S. S. *Inorg. Chem.* **1983**, *22*, 3738.